Microsecond Single-Molecule Tracking (μsSMT) Supplementary Material

S. Semrau, A. Pezzarossa T. Schmidt

December 21, 2010

1 DNA construct

The molecule tracked in the experiments described here was a fluorescently labeled 155 basepair (bp) DNA construct containing a 601 nucleosome positioning sequence [1]. The DNA was prepared by PCR and was labeled with biotin, Cy3B and ATTO647N by incorporation of fluorescently labeled, HPLC purified primers (IBA GmbH). PCR primers were as follows: 5'-TTGG CTGGAGAATC CCGGTGCCGA GGCCGCTCAA TTGGTCGTAG ACAGCTCTAG CACCGCTTAA ACGCACGTAC GCGCTG-3' (Cy3B-labeled nucleotide is underlined) 5'-biotin-TTGGACAGGA TGTATATATC TGACACGTGC CTGGAGACTA GGGAGTAATC CCCTTGGCGG TTAAAACGCG GGGGACAGC-3' (ATTO647N-labeled nucleotide is underlined) In the DNA the Cy3B and the ATTO647N were located 76 bp (24 nm) apart. Since this distance was significantly bigger than the Förster radius of the fluorophores ($\approx 5.5nm$) there was no FRET as confirmed by FCS experiments (data not shown).

2 Single-molecule microscopy

The experimental setup for single-molecule imaging has been described in detail previously [2]. Briefly, the microscope (Axiovert 100; Zeiss, Oberkochen Germany) was equipped with a 100x oil-immersion objective (NA=1.4, Zeiss, Oberkochen, Germany). The samples were illuminated for $t_{\mathrm{ill}} = 1ms$, $3ms$ or $5ms$ by an Ar^+ laser (Spectra Physics, Mountain View, CA, USA) with a wavelength of $514nm$ and a 30mW diode laser (Power technology, Alexander AR, USA) with a wavelength of $639nm$. The length of the laser pulses t_{ill} and the time lag between the pulses Δt were set by an acousto-optical tunable filter (AOTF). The illumination intensity was set to $3\pm0.3\,\mathrm{kW/cm^2}$ for both lasers. A circular diaphragm was introduced in the back focal plane of the tube lens to confine the illumination area and create a flat laser illumination profile. An appropriate filter combination (dichroic Z405/514/647/1064rpc and emission filter Z515/647m, Chroma Technology, Brattleboro,USA) permitted the detection of individual fluorophores by a liquid nitrogen cooled slow-scan CCD camera system (Princeton Instruments, Trenton, NY, USA). The time between two sets

of laser pulses was limited by the readout time of the CCD chip, which was about $290ms$. A dichroic wedge diverted the emitted light to two different regions of the CCD according to emission wavelength, see Fig. 1. In this way the fluorescence signals from the Cy3B and ATTO647N molecules were separated. For the observation of the diffusion of single DNA molecules in solution, the molecules were dissolved in phosphate buffered saline (PBS: 150mM NaCl, 10mM Na_2HPO_4/NaH_2PO_4, pH 7.4), 5% dextran T500 / PBS or 10% dextran T500 / PBS. $1ml$ of the solution was placed on a cover slip in a custom made sample holder and the focus of the microscope was set several μm into the solution (depth of focus $\approx 1\mu m$). The number of molecules in the focal volume was chosen so low that individual fluorophores could be resolved. For each time lag approximately 5000 images were taken (in both color channels), which resulted in the measurement of about 10000-20000 diffusion steps. For typical raw data see the supplementary movie ($t_{\text{ill}} = 5ms$, $\Delta t = 200\mu s$).

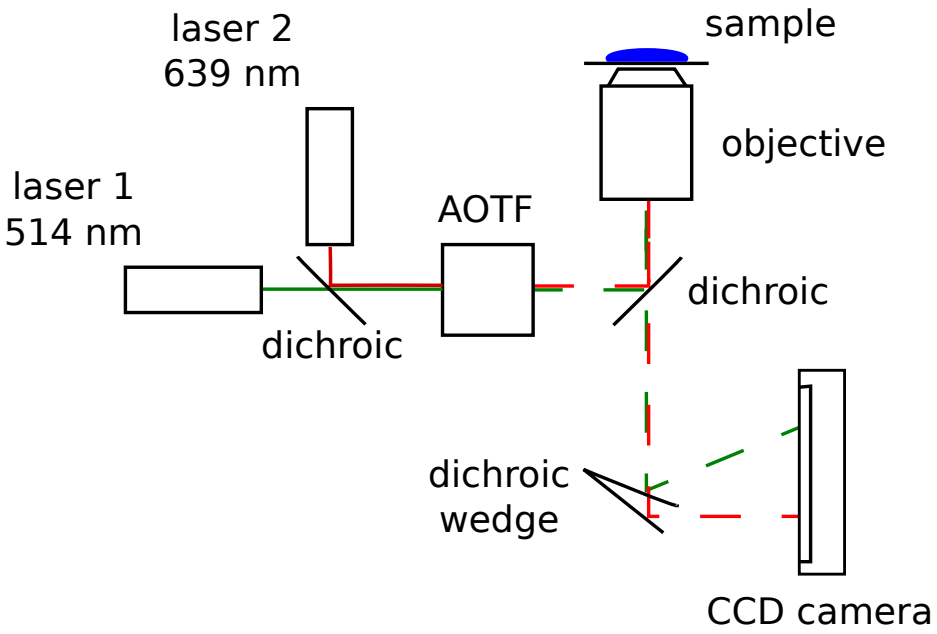

Figure 1: Microscope setup. Two lasers ($514nm$ and $639nm$) were focused on the backfocal plane of a high NA objective which resulted in widefield illumination of the sample. The fluorescence light from the red and green fluorophores respectively was split by a dichroic wedge and directed to different regions on the CCD chip. The two lasers were pulsed independently by an AOTF.

3 Derivation of theoretical result for the averaged MSD

We assume the stochastic process underlying the random walk of the observed molecules is ergodic, which means that the ensemble average $< \ldots >$ is identical to the time average, which is the experimentally accessible quantity. In the following the overline denotes the average over the illumination time.

$$
\begin{aligned}
&\overline{\mathrm{MSD}}(\Delta t) \\
&= \left\langle \left(\overline{\mathbf{r}(t+\Delta t)} - \overline{\mathbf{r}(t)} \right)^2 \right\rangle \\
&= \left\langle \left(\frac{1}{t_{\mathrm{ill}}} \int_{-t_{\mathrm{ill}}}^{0} d\tilde{t}\ \mathbf{r}\left(t+\Delta t+\tilde{t}\right) - \frac{1}{t_{\mathrm{ill}}} \int_{-t_{\mathrm{ill}}}^{0} dt'\ \mathbf{r}\left(t+t'\right) \right)^2 \right\rangle \\
&= \frac{1}{t_{\mathrm{ill}}^2} \int_{-t_{\mathrm{ill}}}^{0} d\tilde{t} \int_{-t_{\mathrm{ill}}}^{0} dt' \left\langle \left(\mathbf{r}(t+\Delta t+\tilde{t}) - \mathbf{r}(t+t')\right)^2 - \mathbf{r}^2(t+\Delta t+\tilde{t}) - \mathbf{r}^2(t+t') \right. \\
&\qquad \left. + \mathbf{r}(t+t')\mathbf{r}(t+\tilde{t}) + \mathbf{r}(t+\Delta t+\tilde{t})\mathbf{r}(t+\Delta t+t') \right\rangle
\end{aligned}
$$

In the last step we expanded the brackets, regrouped the terms and switched the time integral with taking the ensemble average, which is admissible because taking the ensemble average is a linear operation. We further assume that the stochastic process is second-order stationary, i.e.

$$\langle \mathbf{r}(\tau)\mathbf{r}(\tau') \rangle = \langle \mathbf{r}(\tau+a)\mathbf{r}(\tau'+a) \rangle$$

such that

$$
\begin{aligned}
&\overline{\mathrm{MSD}}(\Delta t) \\
&= \frac{1}{t_{\mathrm{ill}}^2} \int_{-t_{\mathrm{ill}}}^{0} d\tilde{t} \int_{-t_{\mathrm{ill}}}^{0} dt' \left\langle \left(\mathbf{r}(\Delta t+\tilde{t}) - \mathbf{r}(t')\right)^2 \right\rangle - \left\langle \left(\mathbf{r}(\tilde{t}) - \mathbf{r}(t')\right)^2 \right\rangle \\
&= \frac{1}{t_{\mathrm{ill}}^2} \int_{-t_{\mathrm{ill}}}^{0} d\tilde{t} \int_{-t_{\mathrm{ill}}}^{0} dt' \left\langle \left(\mathbf{r}(\Delta t+\tilde{t}-t') - \mathbf{r}(0)\right)^2 \right\rangle - \left\langle \left(\mathbf{r}(\tilde{t}-t') - \mathbf{r}(0)\right)^2 \right\rangle \\
&= \frac{1}{t_{\mathrm{ill}}^2} \int_{-t_{\mathrm{ill}}}^{0} dt' \int_{-t_{\mathrm{ill}}-t'}^{-t'} d\varepsilon\ \left(\mathrm{MSD}(\Delta t+\varepsilon) - \mathrm{MSD}(\varepsilon)\right) \quad \text{with} \quad \varepsilon := \tilde{t} - t' \quad , \quad d\varepsilon = d\tilde{t}
\end{aligned}
$$

For normal, two-dimensional diffusion $\mathrm{MSD}(\tau) = 4D\,|\tau|$.

$$
\begin{aligned}
&\overline{\mathrm{MSD}}(\Delta t) \\
&= \frac{4D}{t_{\mathrm{ill}}^2} \int_{-t_{\mathrm{ill}}}^{0} dt' \int_{-t_{\mathrm{ill}}-t'}^{-t'} d\varepsilon\ |\Delta t+\varepsilon| - |\varepsilon|
\end{aligned}
$$

$$I_1 := \int_{-t_{\mathrm{ill}}}^{0} dt' \int_{-t_{\mathrm{ill}}-t'}^{-t'} d\varepsilon\ |\varepsilon| = \int_{-t_{\mathrm{ill}}}^{0} dt'\ \frac{1}{2}\left[(t_{\mathrm{ill}}+t')^2 + (t')^2\right] = \frac{1}{3}t_{\mathrm{ill}}^3$$

$$I_2 := \int_{-t_{\rm ill}}^{0} dt' \int_{-t_{\rm ill}-t'}^{-t'} d\varepsilon \ |\Delta t + \varepsilon|$$

For $\Delta t > t_{\rm ill}$ it holds that $\Delta t + \varepsilon > 0$ since $-t_{\rm ill} \leq \varepsilon \leq t_{\rm ill}$, so

$$I_2 = \Delta t \, t_{\rm ill}^2 + \int_{-t_{\rm ill}}^{0} dt' \int_{-t_{\rm ill}-t'}^{-t'} d\varepsilon \ \varepsilon = \Delta t \, t_{\rm ill}^2$$

For $\Delta t \leq t_{\rm ill}$

$$\begin{aligned} I_2 &= \int_{-t_{\rm ill}}^{0} dt' \int_{-t_{\rm ill}-t'+\Delta t}^{-t'+\Delta t} dz \ |z| \quad \text{with} \quad z := \Delta t + \varepsilon \quad , \quad dz = d\varepsilon \\ &= \int_{-t_{\rm ill}}^{\Delta t - t_{\rm ill}} dt' \int_{-t_{\rm ill}-t'+\Delta t}^{-t'+\Delta t} dz \ z + \int_{\Delta t - t_{\rm ill}}^{0} dt' \left(\int_{-t_{\rm ill}-t'+\Delta t}^{0} dz \ (-z) + \int_{0}^{-t'+\Delta t} dz \ z \right) \\ &= -\frac{1}{3}\Delta t^3 + \Delta t^2 \, t_{\rm ill} + \frac{1}{3} t_{\rm ill}^3 \end{aligned}$$

Combining these terms we arrive at

$$\overline{\rm MSD}(\Delta t) = \frac{4D}{t_{\rm ill}^2} \left(I_2 - I_1 \right) = 4D \times \begin{cases} \left(\frac{\Delta t^2}{t_{\rm ill}} - \frac{1}{3} \frac{\Delta t^3}{t_{\rm ill}^2} \right) & \text{for} \quad \Delta t \leq t_{\rm ill} \\ \left(\Delta t - \frac{1}{3} t_{\rm ill} \right) & \text{for} \quad \Delta t > t_{\rm ill} \end{cases}$$

Due to the finite positional accuracy there is an additional constant term which equals $2(\sigma_{\rm Cy3B}^2 + \sigma_{\rm ATTO647N}^2) =: 4\sigma^2$, where $\sigma_{\rm Cy3B}$ and $\sigma_{\rm ATTO647N}$ are the one-dimensional positional accuracies for Cy3B and ATTO647N respectively. The theoretical expression derived above plus the constant offset $4\sigma^2$ was fit to the experimentally obtained MSD with free fit parameters D and σ. The fit was a weighted least-squares fit with the inverse square root of the errors of every data point as weights. On average $\sigma = 46nm$. For the purpose of better comparability the offsets $4\sigma^2$ were subtracted in Fig. 2 in the main text. The value for σ reported here is comprised of 1. a contribution due to the finite accuracy for the position determination by Gaussian fitting and 2. remaining chromatic aberration which has not been corrected for completely. Chromatic aberration was corrected for with an accuracy of approximately $10nm$ (see below).

4 Fitting of single-molecule signals

Details about finding and fitting single-molecule signals were described elsewhere [3, 4]. Briefly, raw images were filtered with a two-dimensional Gaussian whose width corresponds to the width of the point spread function (PSF) of the microscope. This procedure optimized the signal to noise ratio. The positions of the pixels whose value after filtering exceeded a certain multiple of the noise were used as initial values for the fitting of a two-dimensional Gaussian in the unfiltered image. This thresholding procedure separated true single-molecule signals from noise. From the Gaussian fit, position, width and integrated intensity of the single molecule signal were determined.

5 Correction for chromatic aberration

To achieve an exact spatial correlation between the two detection channels we imaged a fluorescent bead which could be detected in both channels. The bead was adsorbed to a coverslip and moved through the whole region of interest. The positions of the bead in the Cy3B channel $\mathbf{r}_i^{\text{green}}$ and the the ATTO647N channel $\mathbf{r}_i^{\text{red}}$ were determined as described in the previous section. To interpolate the shift for areas which had not been covered by the bead fifth-order polynomials $f_x(\mathbf{r})$ and $f_y(\mathbf{r})$ were fit to the measured positions (separately for the two directions x and y) such that

$$\sum_i (f_x(\mathbf{r}_i^{\text{green}}) - (x_i^{\text{red}} - x_i^{\text{green}}))^2 = \text{minimal !}$$
$$\sum_i (f_y(\mathbf{r}_i^{\text{green}}) - (y_i^{\text{red}} - y_i^{\text{green}}))^2 = \text{minimal !}$$

$f_x(\mathbf{r})$ and $f_y(\mathbf{r})$ then gave the corrective shifts – in x and y respectively– to be applied to a position $\mathbf{r}$ measured in the green channel. Fig. 1d in the main text shows an example for these shifts. To quantify how accurately the described procedure eliminated chromatic aberration we applied the corrective shifts $f_x(\mathbf{r})$ and $f_y(\mathbf{r})$ to the positions of the multifluorescent bead used to measure those shifts. From the remaining differences between the positions in the two color channels we calculated that chromatic aberration was eliminated down to a length scale of approximately $10nm$.

6 Quantification of microscope stage drift

To exclude that drift of the microscope stage influenced the measurements we measured the MSD of fluorescent beads adhered to a cover slip, see Fig. 2. We found that the stage drift (diffusion coefficient $D = 3.1 \pm 1.4 \cdot 10^{-6} \mu m^2/s$) is negligible on the time scale relevant for our experiments ($< 100ms$).

7 Particle Image Cross-Correlation Spectroscopy (PICCS)

PICCS calculates the correlation function between two different types of signals termed "green" and "red" without loss of generality. The PICCS algorithm illustrated in Fig. 3 results in the cumulative correlation function $C_{\text{cum}}(l, \Delta t)$ where Δt is the time-lag between the illumination of the two probes.

If, per image, there is exactly one pair of correlated signals the correlation function $C_{\text{cum}}(l, \Delta t)$ equals $P_{\text{cum}}(l, \Delta t)$, the probability for finding a distance smaller than l between a green and a red signal. If only for a fraction α of all green signals there is a correlated red signal, we observe $C_{\text{cum}}(l, \Delta t) = \alpha P_{\text{cum}}(l, \Delta t)$. Typically there is more than one green signal per image and therefore also more than one red

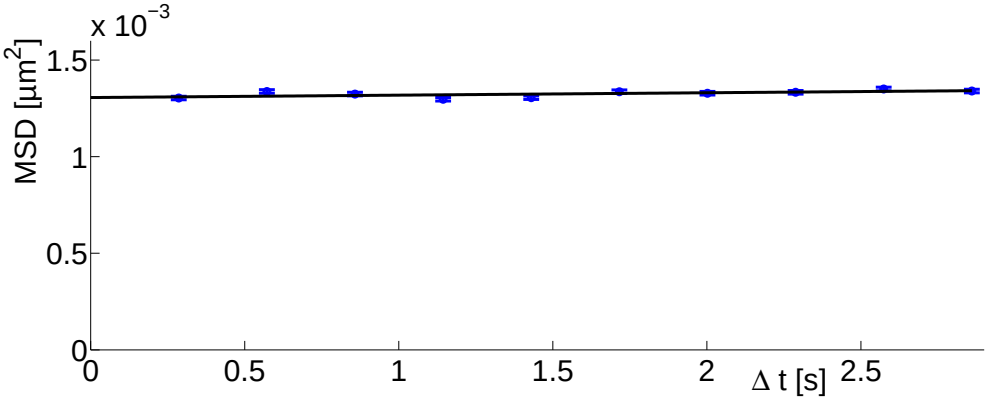

Figure 2: MSD of fluorescent beads adhered to a cover slip (blue circles). The data is fit by a linear diffusion model (solid black line) with a diffusion coefficient of $D = 3.1 \pm 1.4 \cdot 10^{-6} \mu m^2/s$ and a positional accuracy of $18nm$

signal. If l gets bigger, neighboring red signals in close proximity are counted by the PICCS algorithm although they are not correlated with the green signal. Additionally there might be red signals which are not correlated with any green signal at all. These red signals, in close proximity or not correlated with any green signal, lead to an additional contribution $c_{\mathrm{red}} \cdot \pi l^2$ to $C_{\mathrm{cum}}(l, \Delta t)$ – under the assumption that the positions of the red signals follow a uniform random distribution with density c_{red}. In total $C_{\mathrm{cum}}(l, \Delta t) = \alpha P_{\mathrm{cum}}(l, \Delta t) + c_{\mathrm{red}} \cdot \pi l^2$.

If there are no red signals in addition to the ones correlated with a green one, c_{red} can be calculated from the density of green signals c_{green}, the correlation fraction α and the image area A by

$$c_{\mathrm{red}} = \alpha(c_{\mathrm{green}} A - 1)/A = \alpha(c_{\mathrm{green}} - 1/A) \equiv c^*_{\mathrm{red}} \tag{1}$$

If $1/A \ll c_{\mathrm{green}}$, $c_{\mathrm{red}} \approx \alpha c_{\mathrm{green}}$. In general $c_{\mathrm{red}} = c^*_{\mathrm{red}} + c_{\mathrm{red,uncorr.}}$, where $c_{\mathrm{red,uncorr.}}$ is the density of red signals which are not correlated with any green signal.

In practice $P_{\mathrm{cum}}(l, \Delta t)$ is retrieved by subtraction of the linear part of $C_{\mathrm{cum}}(l, \Delta t)$ when plotted against l^2 and subsequent normalization to 1, see Fig. 4

Since the probability to find exactly the distance l between a green and a red signal is $\partial P_{\mathrm{cum}}(l, \Delta t)/\partial l$ the MSD could in principle be calculated by $\overline{\mathrm{MSD}}(\Delta t) = \int_0^\infty dl \; l^2 \partial P_{\mathrm{cum}}(l, \Delta t)/\partial l$. Due to noise this direct calculation would lead to large errors. Instead the heuristic formula

$$P_{\mathrm{cum}}\,(l, \Delta t) = \beta \left(1 - \exp\left(-\frac{l^2}{2\,\mathrm{sd}_1(\Delta t)^2}\right)\right) + (1-\beta)\left(1 - \exp\left(-\frac{l^2}{2\,\mathrm{sd}_2(\Delta t)^2}\right)\right) \tag{2}$$

was fit to $P_{\mathrm{cum}}(l, \Delta t)$ with 3 fit parameters β, $\mathrm{sd}_1(\Delta t)$ and $\mathrm{sd}_2(\Delta t)$, which gave a good description of the data in all cases and eliminated high-frequency noise, see Fig. 4b. The MSD is then simply $\overline{\mathrm{MSD}}(\Delta t) = \beta\,\mathrm{sd}_1(\Delta t)^2 + (1-\beta)\,\mathrm{sd}_2(\Delta t)^2$.

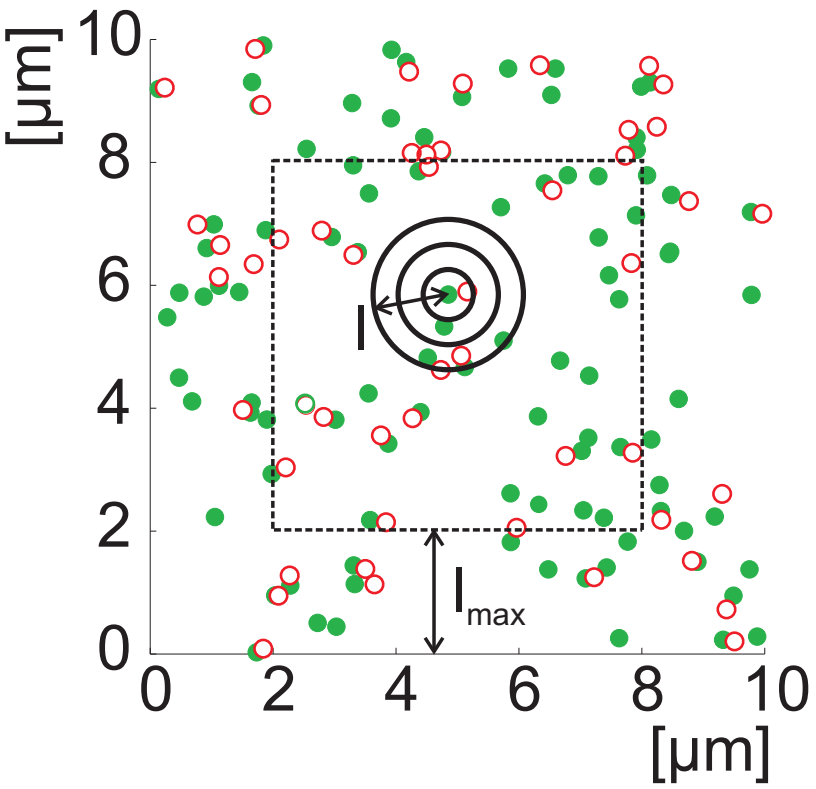

Figure 3: PICCS algorithm. For all green signals (solid circles) the number of red signals (open circles) are counted which fall into a circle of radius l from a green signal. The total number is divided by the number of green signals. By increasing l from 0 to $l_{\max}$ the whole correlation function $C_{\mathrm{cum}}(l, \Delta t)$ is constructed. To avoid edge effects, only the green signals in the area bounded by the dashed line are used. Those signals lie farther away from the edges of the image than the maximal distance $l_{\max}$ analyzed Here $l_{\max} = 2\mu m$. The signal positions were simulated with these parameters: density of green signals $c_{\mathrm{green}} = 1\mu m^{-2}$, correlation fraction $\alpha = 0.5$ (results in a density of red signals of $c_{\mathrm{red}} = 0.5\mu m^{-2}$), correlation length $\sigma = 150nm$.

Finally we have to take into consideration that the positions of single-molecules can be determined only with a finite positional accuracy. The probability $P(\xi, \eta, \Delta t)$ to observe two correlated signals separated by a vector (ξ, η) is the convolution of the real probability $P_{\mathrm{real}}(\xi, \eta, \Delta t)$ and the probability density $P_{\mathrm{pos.acc.}}(\xi, \eta)$ describing the (apparent) correlation due to the finite positional accuracy [5].

$$P(\xi, \eta, \Delta t) = \int\int d\xi'\, d\eta' P_{\mathrm{real}}(\xi - \xi', \eta - \eta', \Delta t) P_{\mathrm{pos.acc.}}(\xi', \eta')$$
$$P_{\mathrm{pos.acc.}}(\xi, \eta) = \frac{1}{2\pi\sigma^2} \exp\left(-\frac{\xi^2 + \eta^2}{2\sigma^2}\right) \tag{3}$$

where $\sigma = \sqrt{2}\sigma_{\mathrm{pos.acc.}}$ and $\sigma_{\mathrm{pos.acc.}}$ is the one-dimensional positional accuracy. For

simplicity we assume here that the positional accuracy is the same for both types of signals. The cumulative probability $P_{\mathrm{cum}}(l, \Delta t)$ is then found by integration of $P(\xi, \eta, \Delta t)$ in polar coordinates

$$P_{\mathrm{cum}}(l, \Delta t) = \int_0^l dr\, r \int_0^{2\pi} d\phi P(r, \phi, \Delta t) \tag{4}$$

with $r = \sqrt{\xi^2 + \eta^2}$, $\phi = \arctan(\eta/\xi)$.

The MSD calculated from this cumulative probability has a constant contribution $4\sigma^2$ [5] as already mentioned above.

8 Error determination

The errorbars in Fig. 2 in the main text were determined from Monte Carlo simulations of the probability $P_{\mathrm{cum}}(l, \Delta t)$ with exactly the same parameters as found in the experiments and the number of molecule positions actually recorded. For each simulation the MSD was determined as described in the previous section and the standard deviation calculated from 100 simulations run with identical parameters.

9 FCS measurements

FCS measurments were performed on a home-made confocal microscope described in detail elsewhere [1]. The measured auto-correlation curves $G(\tau)$ were fit to a model for 3D diffusion.

$$G(t) = \frac{G_0}{(1 + \tau/\tau_d)\sqrt{(1 + (a^{-2})(\tau/\tau_d))}}$$

with the free parameters G_0, the auto-correlation amplitude, a, a geometric factor equal to the ratio of width and height of the focal volume, and τ_d, the diffusion time. First, this expression was fit to the auto-correlation curves for the three different types of solvents (PBS, 5% dextran, 10% dextran) leaving all parameters free. Then parameter a was fixed to the average over the values obtained from the 3 auto-correlation curves. Finally, Eq. 9 was fit again to all auto-correlation curves with G_0 and τ_d as free parameters, which led to the ratios of diffusion times reported in the main text. Errors were determined as errors of the fit of the model to the measured curves. Fig. 5 shows the measured auto-correlation curves and fits of Eq. 9.

10 Viscosity measurements

Bulk kinematic viscosity measurements were performed with a Cannon-Ubbelohde viscometer (CANNON Instrument Company,State College, PA, USA). Measurements of all different solvents used were conducted in triplicates and the error determined as the standard deviation.

References

[1] W. J. A. Koopmans, R. Buning, T. Schmidt, and J. van Noort. spfret using alternating excitation and fcs reveals progressive dna unwrapping in nucleosomes. *Biophys J*, 97(1):195–204, Jul 2009. doi: 10.1016/j.bpj.2009.04.030.

[2] P. H. M. Lommerse, G. A. Blab, L. Cognet, G. S. Harms, B. E. Snaar-Jagalska, H. P. Spaink, and T. Schmidt. Single-molecule imaging of the h-ras membrane-anchor reveals domains in the cytoplasmic leaflet of the cell membrane. *Biophysical Journal*, 86(1 Pt 1):609–16, Jan 2004. doi: 10.1016/S0006-3495(04)74139-9.

[3] T. Schmidt, G. J. Schütz, W. Baumgartner, H. J. Gruber, and H. Schindler. Imaging of single molecule diffusion. *Proc Natl Acad Sci USA*, 93(7):2926–9, Apr 1996.

[4] S. Semrau and T. Schmidt. Membrane heterogeneity - from lipid domains to curvature effects. *Soft Matter*, 5(17):3174–3186, Jan 2009. doi: 10.1039/b901587f.

[5] D. S. Martin, M. B. Forstner, and J. A Käs. Apparent subdiffusion inherent to single particle tracking. *Biophys J*, 83(4):2109–17, Oct 2002. doi: 10.1016/S0006-3495(02)73971-4.

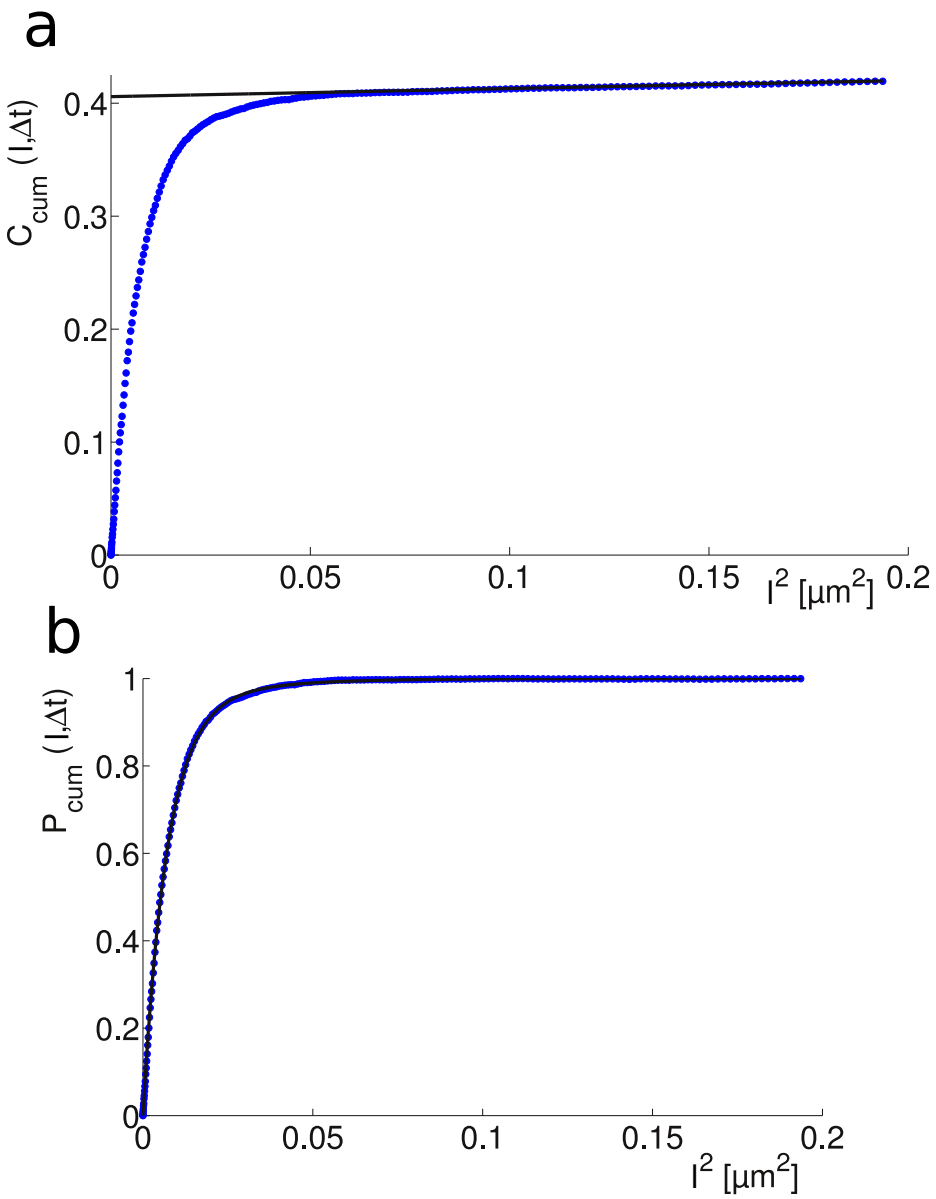

Figure 4: Examples for (a) $C_{\mathrm{cum}}(l, \Delta t)$ and (b) $P_{\mathrm{cum}}(l, \Delta t)$ found in experiments with $\Delta t = 0.3ms$, $t_{\mathrm{ill}} = 3ms$. The solid black line in (a) is a linear fit to the linear part of $C_{\mathrm{cum}}(l, \Delta t)$ plotted against l^2. This linear contribution is subtracted and the resulting curve is normalized to one to obtain $P_{\mathrm{cum}}(l, \Delta t)$ shown in (b). The solid black line in (b) is a fit of Eq. 2 to the data.

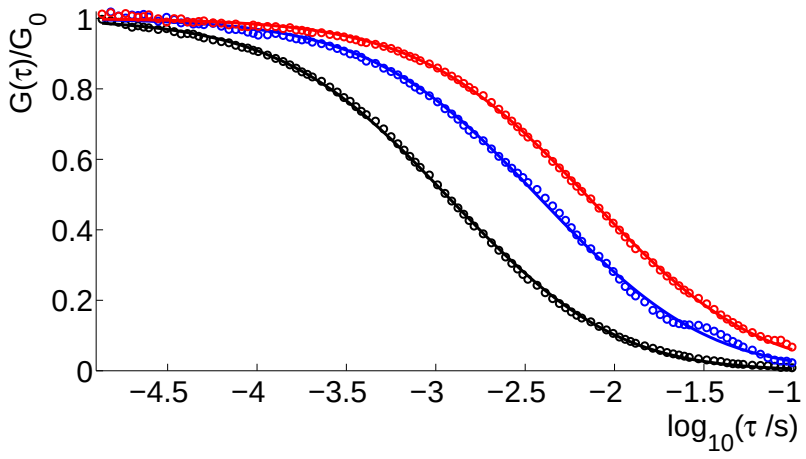

Figure 5: Auto-correlation curves measured by FCS for the DNA oligomer in PBS (black), 5% dextran (blue) and 10% dextran (red). The solid lines are fits of Eq. 9 to the measured auto-correlation curves with G_0 and τ_d as free parameters. For better comparability all auto-correlation curves were normalized to the fitted G_0